The Effect of Varying Jaw-elevator Muscle Forces on a Finite Element Model of a Human Cranium

VIVIANA TORO-IBACACHE[1,2]* **AND PAUL O'HIGGINS**[1]

[1]Centre for Anatomical and Human Sciences, Department of Archaeology and Hull York Medical School, University of York, Heslington, York, YO10 5DD, UK

[2]Facultad De Odontología, Universidad De Chile, Sergio Livingstone Pohlhammer 943, Independencia, Región Metropolitana, Chile

ABSTRACT

Finite element analyses simulating masticatory system loading are increasingly undertaken in primates, hominin fossils and modern humans. Simplifications of models and loadcases are often required given the limits of data and technology. One such area of uncertainty concerns the forces applied to cranial models and their sensitivity to variations in these forces. We assessed the effect of varying force magnitudes among jaw-elevator muscles applied to a finite element model of a human cranium. The model was loaded to simulate incisor and molar bites using different combinations of muscle forces. Symmetric, asymmetric, homogeneous, and heterogeneous muscle activations were simulated by scaling maximal forces. The effects were compared with respect to strain distribution (i.e., modes of deformation) and magnitudes; bite forces and temporomandibular joint (TMJ) reaction forces. Predicted modes of deformation, strain magnitudes and bite forces were directly proportional to total applied muscle force and relatively insensitive to the degree of heterogeneity of muscle activation. However, TMJ reaction forces and mandibular fossa strains decrease and increase on the balancing and working sides according to the degree of asymmetry of loading. These results indicate that when modes, rather than magnitudes, of facial deformation are of interest, errors in applied muscle forces have limited effects. However the degree of asymmetric loading does impact on TMJ reaction forces and mandibular fossa strains. These findings are of particular interest in relation to studies of skeletal and fossil material, where muscle data are not available and estimation of muscle forces from skeletal proxies is prone to error. Anat Rec, 299:828–839, 2016. © 2016 Wiley Periodicals, Inc.

Key words: finite element analysis; human cranium; masticatory muscle activity; sensitivity analysis

Finite element analyses (FEAs) simulating masticatory system loading in crania of primate hominin fossils and modern humans are increasingly common. However data on muscle forces, required to accurately load a model to simulate a particular function are often lacking. This means that approximations and simplifications are required and the sensitivity of finite element models to these needs to be understood. Muscle force is a parameter that is of relevance in any mechanical analysis of the masticatory system. It is generally agreed

that, in simple terms, the human jaw functions as a lever (Hylander, 1975; Koolstra et al., 1988; Spencer, 1998) with the temporomandibular joint (TMJ) acting as a fulcrum, the bite point as the resistance and the muscle force as the load. The magnitude of the resulting bite force is dependent on skeletal anatomy, the locations of muscle attachment sites and so, lever arm lengths as well as muscle force magnitudes. FEA has been increasingly used to predict the mechanical response of the skull to both muscle and bite forces in terms of deformation, strains and stress. These parameters are then commonly investigated in relation to evolutionary (Strait et al., 2009; Wroe et al., 2010; Smith et al., 2015b), developmental (Kupczik et al., 2009) and physiological or pathological processes and adaptations (Tanne et al., 1988; Gross et al., 2001; Koolstra and Tanaka, 2009; Ross et al., 2011; Toro-Ibacache et al., 2016b).

Because reliable FEA simulation depends on accurate geometry and boundary conditions (Richmond et al., 2005; Rayfield, 2007; Kupczik, 2008), anatomically and functionally accurate models should work better than simplified models. However, current methods for FE model construction cannot fully reproduce the details of skull morphology, material properties and functional loadings, particularly when these data are not available as is the situation when dealing with archaeological or fossil material. These cases pose a particular dilemma in estimating muscle forces, which raises the question of the effects of inaccurate muscle force estimation on FE model performance. Many sensitivity analyses have been carried out in relation to FEA of vertebrate crania or mandibles. These have mainly focused in the effects of omitting anatomical structures such as sutures, sinuses, the periodontal ligament, or on the effects of varying the mechanical properties of bone (Strait et al., 2005; Kupczik et al., 2007; Gröning et al., 2011; Wood et al., 2011; Bright, 2012; Fitton et al., 2015). Only two articles have assessed the effects of varying muscle parameters on the strains/stresses of FE models of non-human primate crania (Ross et al., 2005; Fitton et al., 2012). In both cases, the authors concluded that although the varying of muscle parameters impacts performance, the importance of the effects should be weighed against the aims of the study. Here we aim to systematically explore the impact of errors in applied muscle forces in an FE model of a modern human cranium to better understand the consequences in hominins.

The maximum contractile force of a muscle can be estimated using anatomical and chemical dissection methods to measure muscle mass and fiber length and so, to estimate muscle physiological cross-sectional area (van Eijden et al., 1997; Antón, 1999) which is directly proportional to the maximum force that can be generated. This method is impractical for ethical reasons in living humans, and impossible in archaeological and fossil material. In living humans, the cross-sectional areas (CSA) of jaw-elevator muscles obtained from medical images have been proposed as a reasonable estimator of the potential maximum force of pennate muscles (Weijs and Hillen, 1985, 1986; Koolstra et al., 1988; van Spronsen et al., 1991). When the muscles are absent, like in fossil or museum material, bony marks are used to estimate CSA (Demes and Creel, 1988; Antón, 1990; O'Connor et al., 2005; Wroe et al., 2010). However, we showed in a previous study that the CSA estimation based on

bone markings is not accurate in humans, leading to an overestimation of force magnitudes and, in the case of the masseter, values that do not correlate with the measured ones (Toro-Ibacache et al., 2015).

Estimating the magnitude of force actually produced by a muscle during a certain task can also pose a challenge. The electromyographic (EMG) activity of a muscle while exerting maximum and sub-maximum voluntary contractions is often used as a proxy for muscle force (Hagberg et al., 1985; Ueda et al., 1998; Farella et al., 2009). When maximum muscle forces are estimated from muscle PCSAs, the normalized levels of EMG activity can be used to scale the force magnitudes produced under a certain task (see Ross et al., 2005 for a study in *Macaca*). This approach is limited to superficial muscles unless invasive methods are used (Soderberg and Cook, 1984; Reaz et al., 2006), which constrains its use in living humans. Although the EMG activity of masticatory muscles has a complex relationship with bite force, during isometric contraction a close-to-linear relationship is found (Prum et al., 1978; Hagberg et al., 1985; Wang et al., 2000). During biting tasks, a symmetric pattern of activation has been observed during maximum intercuspidation (Ferrario et al., 2000; Schindler et al., 2005), unilateral food crushing (Spencer, 1998) and isometric bites (van Eijden, 1990) but not during complete, consecutive mastication cycles (Stohler, 1986). Additionally, Farella et al. (2009) found changing patterns of muscle activation over time under maximum and sub-maximum sustained unilateral bites. Intra and inter-individual variability in muscle force levels is then an additional source of complexity in data reproduction.

The effects of incorrectly reproducing the magnitudes of masticatory muscle forces on reaction forces and the mode and magnitude of deformation predicted by FE models of the human cranium have not yet been explored, and is the aim of the present study. Deformation is assessed both locally using strains and globally (i.e., general changes in size and shape) using geometric morphometric methods (Fitton et al., 2012; O'Higgins and Milne, 2013).

We tested the hypothesis that varying the relative magnitudes of muscle force during the same biting task has no effect on FEA results in terms of strain distribution and magnitudes, bite forces, TMJ reaction forces, and global modes of model deformation. To test this hypothesis, several extreme combinations of muscle forces representing different patterns of muscle activation were simulated while skull and muscle anatomy, tissue material properties and the kinematic constraints of the model were kept constant. It is to be expected from Hooke's law that principal strain magnitudes will scale linearly with applied total load (O'Higgins and Milne, 2013), however the expectations with regard to modes of deformation are less clear.

MATERIALS AND METHODS

Data

An FE model of the cranium of a male human aged 43, with full dentition, was built from segmented CT data used in previous studies (Toro-Ibacache et al., 2015; Toro-Ibacache et al., 2016b), where muscle CSAs were also directly measured. The image data comprise a medical CT scan of a living patient taken at the Teaching

Hospital of the University of Chile (Hospital Clínico de la Universidad de Chile, Santiago de Chile). The data were used with ethics committee approval, under the terms of the hospital ethics protocol for the use of patient data. The CT scan was carried out for medical reasons before the beginning of this study using a Siemens 64-channel multidetector CT scanner equipped with a STRATON tube (Siemens Somatom Sensation 64, Siemens Healthcare, Erlangen, Germany). The primary reconstruction of images was performed using specialist software tool (Syngo Multimodality Workplace, Siemens Healthcare, Erlangen, Germany). Voxel size was $0.44 \times 0.44 \times 1$ mm^3. The segmentation was performed on the image stacks exported as DICOM files.

Three-dimensional cranial morphology was reconstructed from the CT volume stack using Avizo (v.7.0.1, Visualization Sciences Group, Burlington, USA). Semi-automated segmentation of CTs based on grey level thresholds was used to separate bone from surrounding tissues and air. Manual segmentation was then performed where needed for anatomical accuracy. Paranasal sinuses were preserved but cortical and cancellous bone were not segmented as distinct tissues, rather the bone was treated as a solid whole with the material properties of cortical bone. This approach has been used in a macaque model (Fitton et al., 2015) and validated in a previous study (Toro-Ibacache et al., 2016a) that showed little effect on mode of deformation (the key focus of this study).

Finite Element Model and Loadcases

The volume data produced by the CT segmentation was resampled to an isometric voxel size of 0.44 mm, exported as BMP stacks and converted into an FE mesh of 6,306,181 eight-noded cubic elements by direct voxel conversion. Cancellous bone was omitted, and hence all bone was modelled as a solid material with a Young's modulus of 17 and 50 GPa for teeth, both with a Poisson's ratio of 0.3. This model building approach has been used in previous studies of cranial FE models (Wroe et al., 2010; Bright and Gröning, 2011; Fitton et al., 2012; Jansen van Rensburg et al., 2012; Toro-Ibacache et al., 2016b) and is relevant in cases where model resolution, fossilization or taphonomic processes do not allow to accurately model cancellous bone (Bright and Gröning, 2011; Fitton et al., 2015; Toro-Ibacache et al., 2016b), or when models are generated via 3D surface warping (O'Higgins et al., 2011).

Each loaded model was kinematically constrained at the most anterior and superior parts of both mandibular fossae in the x, y, and z axes. Vertical constraints on the incisal border of both central incisors (I^1) and on the occlusal face of left and right first molars (M^1) were applied separately, simulating bite points. The choice of axes of constraint was based on prior experiments in which constraints were reduced (e.g., TMJ constrained in x and y only) with the result that the model experienced rigid-body motion when loaded. Thus the chosen constraints were the minimum required to fix the model in space while not over-constraining it. Left and right M^1 bites were simulated to control for possible effects of asymmetries in bone morphology and muscle attachment. Muscle origins and insertions were reproduced in

TABLE 1. Estimated values of CSA and maximum forces of jaw-elevator muscles

Muscle	CSA (cm^2)		Muscle force (N)	
	Left	Right	Left	Right
Temporalis	4.54	4.61	168.02	170.67
Masseter	3.62	3.35	134.06	124.01
Medial Pterygoid	3.35	3.18	124.01	117.49

the model based on the original CT image in which muscles were clearly visible.

Muscle Forces

Static bites were simulated at I^1 and unilaterally at the left or right M^1. As noted above, the maximum muscle forces from the temporal, masseter and medial pterygoid muscles were estimated from their CSAs measured in previous studies (Toro-Ibacache et al., 2015; Toro-Ibacache et al., 2016b) using a protocol based on that of Weijs and Hillen (1984) and the formula, Force = CSA $\times$ 37 N cm^{-2}, where the last term is an estimate of the magnitude of intrinsic muscle strength for human masticatory muscles (Weijs and Hillen, 1985; O'Connor et al., 2005). The estimated values of CSA and maximum forces are presented in Table 1.

Before assessing the impact of different loading scenarios on FE model performance, two sensitivity analyses were undertaken. In the first, the results of applying maximal forces based on estimated CSAs, which are asymmetric (Table 1), were compared with identical biting simulations using symmetric muscle forces (average of left and right applied to both sides). In the second, the strain maps resulting from the simulated bites on left and right M1 were compared to check that bites on different sides produce results that are approximately reflected versions of each other.

To test the hypothesis, loadcases simulating different muscle activation levels for each bite point were made by scaling the estimated maximum muscle forces (Ross et al., 2005; Fitton et al., 2012). Because it is impractical to reproduce all possible combinations of muscle forces, three main patterns of "activation" were explored, based on EMG studies of individuals performing different biting tasks. These simulated activation patterns use: symmetric and homogeneously activated muscles during I^1 and unilateral M^1 bites, asymmetric and homogeneously activated muscles during unilateral M^1 bites and symmetric and asymmetric heterogeneously activated muscles under both I^1 and M^1 bites.

To simulate symmetric, homogeneous muscle activations (van Eijden, 1990; Spencer, 1998), the models were loaded during both I^1 and M^1 biting simulations with the forces of the three pairs of jaw-elevator muscles all scaled to 100, 50, or 25% of maximum force.

To simulate asymmetric, homogenously activated muscles during M^1 biting (Blanksma and van Eijden, 1995), each muscle of the working side applied 100% of its maximum force. On the balancing side, the forces applied by each muscle were simultaneously scaled to 75, 50, or 25% of the maximum.

To simulate symmetric, heterogeneously activated muscles (Vitti and Basmajian, 1977; Moore et al., 1988;

TABLE 2. Predicted bite and TMJ reaction forces

Loadcase	Bite point	Working/balancing side muscle activation	Bite force (N)	TMJ reaction force (N)	
				L-TMJ	R-TMJ
1	L- and R-I[1]	100%/100%	234.29	218.76	254.22
2	L- and R-I[1]	50%/50%	117.15	109.38	127.10
3	L- and R-I[1]	25%/25%	58.60	54.67	63.59
4	L-M[1]	100%/100%	358.91	87.77*	277.53
5	L-M[1]	50%/50%	179.44	43.89*	138.75
6	L-M[1]	25%/25%	89.72	21.95*	69.39
7	R-M[1]	100%/100%	355.09	242.91	128.81*
8	R-M[1]	50%/50%	177.58	121.48	64.42*
9	R-M[1]	25%/25%	88.56	61.01	32.36*
10	L-M[1]	100%/75%	315.84	110.69*	205.81
11	L-M[1]	100%/50%	272.73	135.96*	135.74
12	L-M[1]	100%/25%	229.61	162.43*	72.56
13	R-M[1]	100%/75%	309.76	174.33	145.76*
14	R-M[1]	100%/50%	264.27	106.15	166.17*
15	R-M[1]	100%/25%	220.05	39.99	187.86*
16	L- and R-I[1]	50% (T), 100% (M&MP)/50% (T), 100% (M&MP)	188.74	176.31	195.99
17	L- and R-I[1]	25% (T), 100% (M&MP)/25% (T), 100% (M&MP)	165.90	161.85	170.76
18	L-M[1]	50% (T), 100% (M&MP)/50%	237.59	83.94*	146.09
19	L-M[1]	25% (T), 100% (M&MP)/50%	219.99	72.50*	151.36
20	R-M[1]	50% (T), 100% (M&MP)/50%	230.02	120.51	102.51*
21	R-M[1]	25% (T), 100% (M&MP)/50%	212.79	127.75	77.85*

L = left, R = right, T = temporalis, M and MP = masseter and medial pterygoid muscles. TMJ forces from the working side are marked with an asterisk (*).

van Eijden, 1990; Blanksma and van Eijden, 1995; Farella et al., 2009), during I[1] biting the maximum forces of the temporalis, masseter and medial pterygoid were applied in the ratio of 50%:100%:100%, and then 25%:100%:100% of maximum force. In the asymmetric, heterogeneously activated loadcases during M[1] biting simulations, 50% of the maximum force of all balancing side muscles was applied. Two separate sets of working side forces were applied in the following ratios: temporalis:masseter:medial pterygoid = 50%:100%:100% and 25%:100%:100%.

Details of muscle activations in each loadcase are provided in Table 2. Loadcases 1 to 3 simulate symmetric, homogeneous muscle activations under I[1] bites. Loadcases 4 to 9 simulate symmetric, homogeneous activations under left and then right M[1] bites. Loadcases 10 to 15 represent asymmetric, homogenously activated muscles during left and then right M[1] biting. Loadcases 16 and 17 represent symmetric, heterogeneously activated muscles during I[1] biting. Loadcases 18 to 21 simulate asymmetric, heterogeneously activated loadcases during left and then right M[1] bites.

Model pre- and postprocessing were performed using the FEA program VOX-FE (Fagan et al., 2007; Liu et al., 2012).

Comparison of Mechanical Performance among Loadcases

Bite forces and TMJ reaction forces were calculated by summing the forces predicted by the FEA at each constrained node on the tooth. Force magnitudes were then plotted against applied muscle forces to assess the relationships between these variables. Deformation of the model was assessed by comparing strain contour plots, representing the spatial distribution of regions of high and low strains

and their magnitudes. Global modes of deformation were also compared among loadcases using Procrustes size and shape analyses based on a configuration of 51 craniofacial landmarks (Table 3) representing the form of the cranium and facial structures normally strained during biting (Demes, 1987; Gross et al., 2001; Kupczik et al., 2009; Ross et al., 2011). The Procrustes size and shape analysis comprises rotation and translation but not scaling of the landmark coordinates of the original, unloaded cranium and the coordinates from the deformed, loaded crania, followed by principal components analysis (PCA) of the new coordinates (Fitton et al., 2012; O'Higgins et al., 2012). It has been argued (Curtis et al., 2011) that zygomatic arch deformations from primate skull FEA may not accurately reflect reality because the temporalis fascia which is, as in this study often omitted, may limit zygomatic arch deformation in life. Therefore, in order to assess the impact of zygomatic arch deformation on the analysis of global model deformation the size and shape analysis was repeated using a subset of 43 landmarks, excluding those located in the zygomatic arch (see Table 3).

The analysis of global model deformation was performed using the EVAN toolbox (v.1.62, www.evan-society.org).

RESULTS

Before considering the results in relation to the hypothesis, two initial sensitivity analyses are reported. In the first, the results of applying maximum forces based on estimated CSAs, that are asymmetric (Table 1), are compared with identical biting simulations using identical left-right muscle forces (average of left and right, applied to both sides). Compared to the loadcases based on directly estimated (and so, asymmetric) maximum muscle forces, the symmetric loadcases predicted

TABLE 3. Landmarks for size and shape analysis of global deformation

No.	Name	Definition
1	Vertex	Highest point of the cranial vault.
2	Nasion	Intersection between frontonasal and internasal junction.
3	Anterior nasal spine	Tip of the anterior nasal spine.
4	Prosthion	Most buccal and occlusal point of the interalveolar septum between central incisors.
5	Occiput	Most posterior point of the cranium.
6&20	Supraorbital torus	Most anterior point of the supraorbital ridge.
7&21	Infraorbitale	Most inferior point of the infraorbital ridge.
8&22	Nasal notch	Most lateral point of the nasal aperture.
9&23	First molar	Most buccal and mesial point of the junction of M^1 and the alveolar process.
10&24	Last molar	Most buccal and distal point of the junction between the.last molar and the alveolar process.
11&25	Zygo-maxillar	Most inferior point of the zygomatico-maxillary junction.
12&26	Fronto-zygomatic	Most lateral point of the fronto-zygomatic junction.
13&27	Fronto-temporal angle	Point at the intersection between the frontal and temporal processes of the zygomatic bone.
14&28	Zygomatic arch lateral*	Most lateral point on the zygomatic arch.
15&29	Zygomatic aoot posterior	Most posterior-superior point of the intersection between the zygomatic root and the squama of the temporal bone.
16&30	Zygomatic root anterior	Most anterior point of the intersection between the zygomatic root and the squama of the temporal bone.
17&31	Zygomatic arch medial*	Most lateral point on the inner face of the zygomatic arch.
18&32	Infratemporal crest	Most medial point of the infratemporal crest.
19&33	Eurion	Most lateral point of the cranial vault.
34&37	Anterior temporalis origin	Most anterior point of origin of the temporal muscle in the temporal line.
35&38	Superior temporalis origin	Most superior point of origin of the temporal muscle in the temporal line.
36&39	Posterior temporalis origin	Most posterior point of origin of the temporal muscle in the temporal line.
40&43	Anterior masseteric origin	Most anterior point of origin of the masseter muscle.
41&44	Posterior masseteric origin*	Most posterior point of origin of the masseter muscle.
42&45	Mid-Masseteric origin*	Midpoint along the origin area of the masseter muscle.
46&49	Superior pterygoid origin	Most superior point of origin of the medial pterygoid muscle.
47&50	Inferior pterygoid origin	Most inferior point of origin of the medial pterygoid muscle.
48&51	Mid-pterygoid origin	Midpoint of the area of origin of the medial pterygoid muscle.

The landmarks on the zygomatic arch are marked with an asterisk (*).

virtually identical bite forces, TMJ reaction forces and strain magnitudes. With regard to mode of deformation, patterns of strain distribution (data not shown) and global model deformation (see results for all loadcases) assessed by landmarks were also almost identical. In the second sensitivity analysis, bites on left and right M^1 resulted in strain contour maps that are almost perfect mirror images of each other (data not shown). As such, only the strain distributions and magnitudes under left M^1 bites are considered further.

Strain Distribution and Magnitudes

For each simulated bite, the strain contour maps arising from different loadcases show differences in strain magnitudes but much less so in distribution. Thus, where strains are predicted to be relatively high or low differs little among simulations but the average strain magnitude does differ.

The highest strains and largest fields of high strain are found in the regions of masseter and medial pterygoid attachment, and in the facial regions close to the bite point. That is, during incisor bites, the maxilla adjacent to

the nasal notch and, during molar bites, the zygomatic region and frontal process of the maxilla (Figs. 1 and 2).

During I^1 biting simulations, strains decrease from maximum values of >200 µɛ to 100–200 µɛ in the face, zygomatic arch, and mandibular fossae as the magnitude of total applied muscle force decreases. Although this was expected for models 1–3, in the other I^1 loadcases the distribution of regions of high and low strain hardly varies, irrespective of the pattern of muscle activation (Fig. 1). The same situation occurs in the face during unilateral M^1 bites. In the mandibular fossa, strain magnitudes differ between left and right sides among loadcases. The loadcases with more symmetric total muscle forces, that is loadcases 4 to 9 and 18 to 21 (see Table 2 for details), predict the highest strains over the mandibular fossa of the balancing side relative to the working side (e.g., in loadcase 4, strains in the fossae exceed 200 µɛ and are larger on the balancing than on the working side; Fig. 2). This pattern is inverted when the most markedly asymmetric activation patterns are applied (loadcases 11, 12, 14, and 15; Fig. 2). Thus, when the most asymmetric muscle activation pattern is applied (loadcases 12 and 15), the mandibular fossa of the working side shows a larger area reaching strains over 200 µɛ than the balancing side fossa where most strains are ~150 µɛ (Fig. 2).
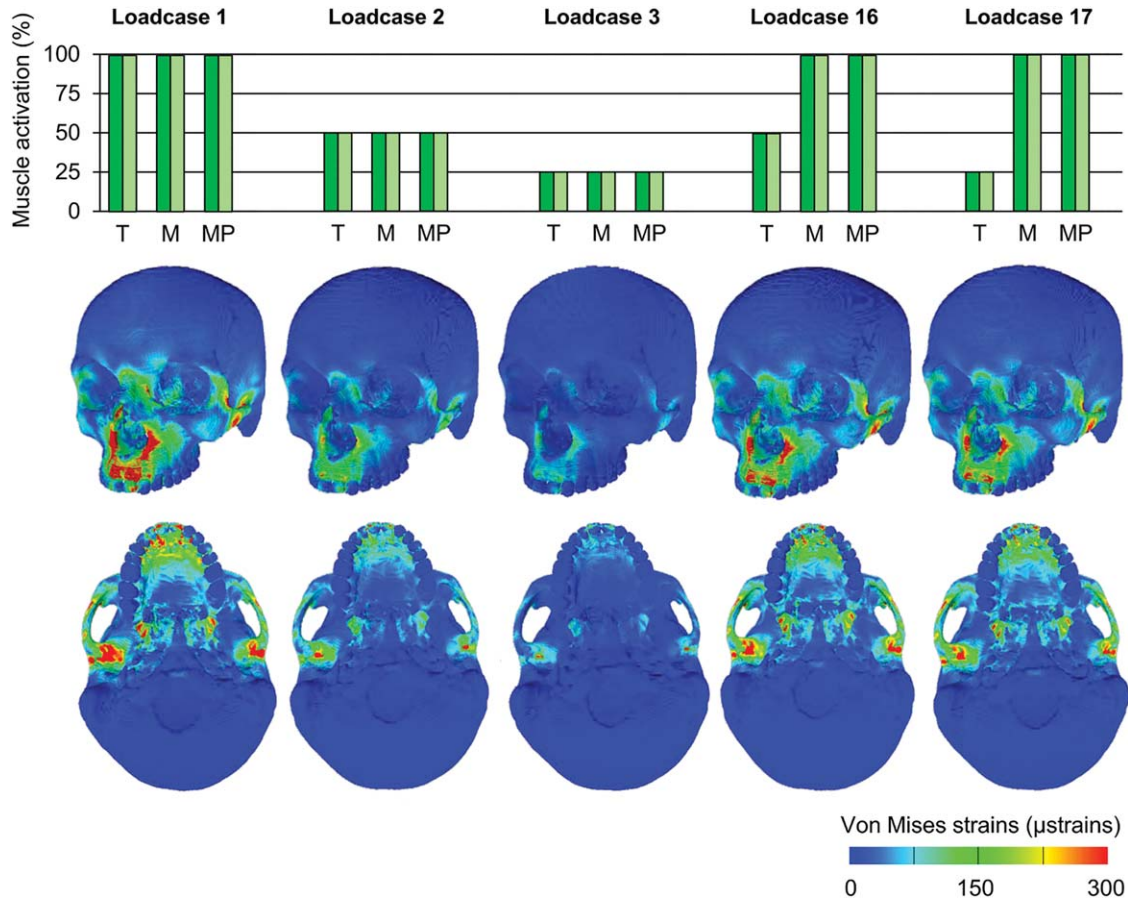
Fig. 1. Strain contour plots from example I^1 biting simulations. The charts depict the percentages of maximal muscle force applied in each loadcase: working side, dark green bars; balancing side, light green bars. Loadcases 1, 2, and 3 correspond to symmetric, homogeneous muscle forces. Loadcases 16 and 17 simulate symmetric, heterogeneous muscle forces, with lower levels of activation of the temporalis (T) compared to masseter (M) and medial pterygoid (MP) muscles.

Bite Force and TMJ Reaction Force

Predicted bite forces and TMJ reaction forces (Table 2; Figs. 3–5) are consistent with the results depicted by the strain contour plots. In general, bite force and TMJ reaction force increase in proportion to total applied muscle force, particularly during I^1 bites (loadcases 1 to 3, 16 and 17; Figs. 3a and 5a). During M^1 bites, TMJ reaction force is higher on the balancing side than the working side with homogeneously activated muscles (loadcases 4 to 9; Figs. 3b,c). In contrast, increasingly asymmetric, homogenous loadcases (10 to 15; Fig. 4) predict lower TMJ forces on the balancing than the working side, and those with asymmetric, heterogeneously activated muscles (i.e., those with varying working side temporalis force, loadcases 18 to 21; Figs. 5b,c) further reduce the TMJ force difference between working and balancing sides.

Global Model Deformation

The Procrustes size and shape PCA of cranial deformations resulting from FEA distinguished three different general vectors of deformation, one for each bite point. These are represented as lines connecting the unloaded model and the loadcases for each bite point (Fig. 6). Differences among loadcases with the same bite point comprise mainly differences in magnitude (distance from the unloaded model) rather than mode (direction of vector). The vectors connecting the unloaded and molar biting simulations are almost symmetrically disposed about the vectors representing incisor bites (Fig. 6). Thus, the global model deformations arising from left and right M^1 bites are almost mirror images of each other. The small degree of asymmetry in the vectors likely reflects asymmetry of form. These findings reflect the symmetries and asymmetries of the strain contour maps noted earlier.

The largest degrees of deformation (distances between unloaded and loaded models in the plot) are achieved when muscles are activated homogeneously and maximally, irrespective of the bite point. Examining the inset warpings, in both I^1 and M^1 bites the greatest deformations occur in the alveolar process near the bite point. With incisor bites the lower face is dorso-ventrally deflected with respect to the upper face and neurocranium. With M^1 bites the face undergoes torsion and local deformation above the bite point. The vectors of
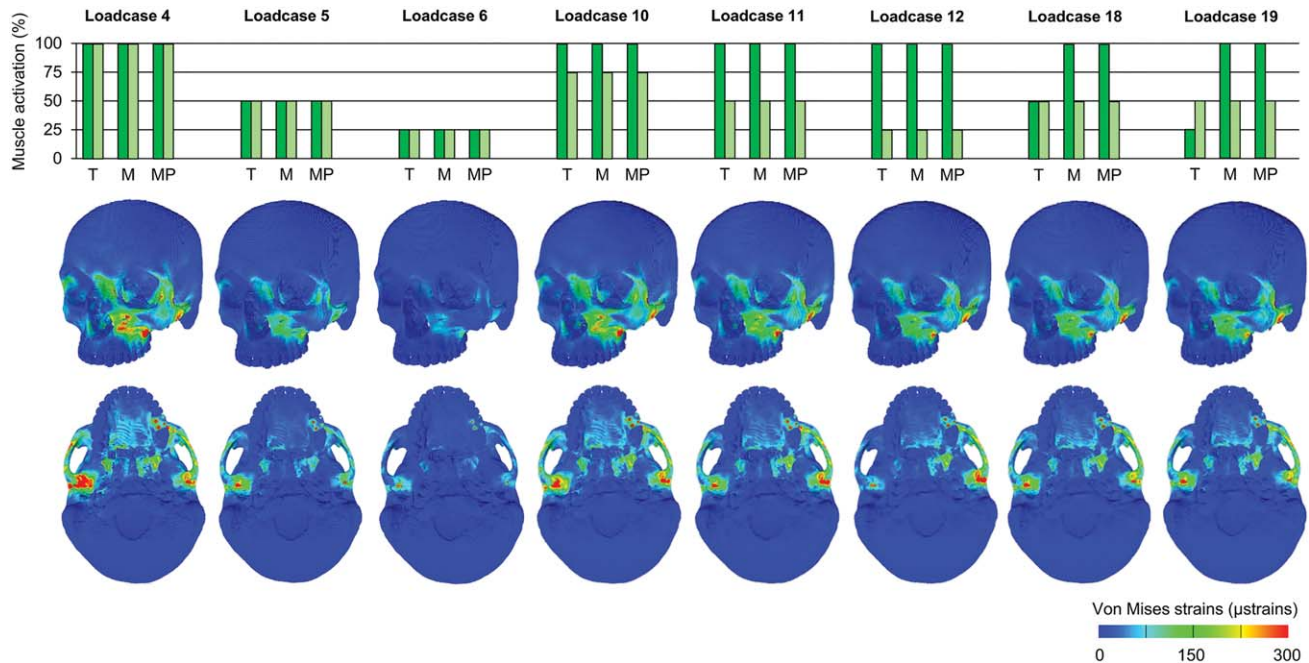
Fig. 2. Strain contour plots from left M[1] biting simulations. The charts depict the percentages of maximal muscle force applied in each loadcase: working side, dark green bars; balancing side, light green bars. Loadcases 4, 5, and 6 correspond to symmetric, homogeneous muscle forces. Loadcases 10, 11, and 12 correspond to asymmetric, homogeneous muscle forces, with diminishing simulated activation of balancing side muscles. Loadcases 18 and 19 simulate asymmetric, heterogeneous muscle forces, with the temporalis (T) activated to lesser degree than masseter (M) and medial pterygoid (MP) muscles on the working side.

deformation of the models with symmetrically applied but varying muscle forces scale exactly in proportion to applied force and are coincident in direction. As noted earlier for strains, loadcases created using perfectly symmetric muscle forces (the average of left and right) deform along almost identical vectors as models using their directly estimated and so, asymmetric force magnitudes (loadcases 1S to 9S, Fig. 6).

The omission of zygomatic arch landmarks has a small effect on the PCA of FEA results (Fig. 7). The main effect is that the vectors from all muscle activation patterns applied to each bite point more nearly overlap. This indicates that deformations of the zygomatic arch accounted for a substantial portion of the divergences between vectors representing the same bite point in Fig. 6.

DISCUSSION

The present study assessed the effects on FE model performance of varying muscle activations during simulated static incisor and molar bites. This is important because muscle forces are rarely known with any precision, and this is especially so when simulating biting in fossil or skeletal material. In consequence, simplified or estimated loadings are often applied. Thus maximal muscle forces might be more or less accurately estimated from bony proxies (Wroe et al., 2010) or estimated from data corresponding to other, related species (Strait et al., 2009; Smith et al., 2015b). Forces might be applied to simulate maximum (100%) activation of all muscles (Smith et al., 2015a) or some more complex muscle activation pattern might be used (Kupczik et al., 2009). This

study aimed to assess the sensitivity of some aspects of FE model performance to such variations in muscle activations; namely strains, bite forces, TMJ forces and global modes of model deformation.

The null hypothesis is that varying the relative magnitudes of muscle force during the same biting task has no effect on FEA results in terms of strain distribution and magnitudes, bite forces, TMJ reaction forces, and global modes of model deformation. Strictly, this hypothesis was falsified, but the effects of varying muscle activation pattern on modes of deformation are very small everywhere except in the zygomatic arch and mandibular fossa. As expected given that bone is represented by an isotropic linearly elastic material, the effect of varying magnitudes of force is to proportionately diminish the magnitude of model deformation. Likewise, bite and TMJ reaction forces also scale with muscle force. These results are further discussed below.

Strain Distribution and Magnitude

During all simulations, strains are greatest in the in the vicinity of the bite point and large where the masseter and medial pterygoid muscles attach. Temporalis, in having a very large attachment area to the large, stiff cranium, does not produce large strains over the vault when it contracts. Thus the major changes in cranial strain maps between muscle activation patterns occur in the regions of the masseter and medial pterygoid attachments.

The results of this study indicate that the greatest impact on facial strains arises through variations in the total applied muscle force. Strain magnitudes (Figs. 1
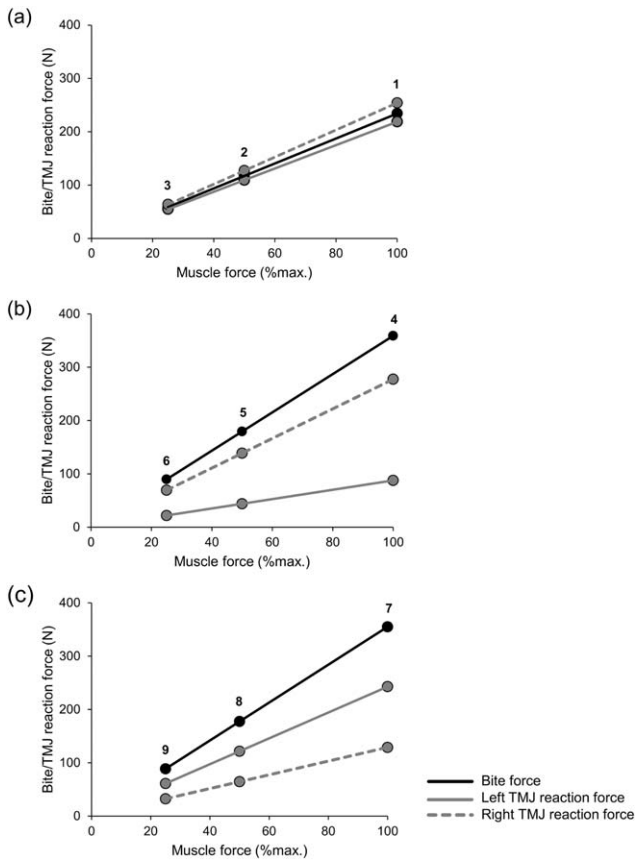
Fig. 3. Bite forces and TMJ reaction forces in loadcases simulating symmetrically and homogeneously activated muscles. Loadcase number is shown in bold. (a) I[1] bites, (b) left M[1] bites (working side = left), and (c) right M[1] bites (working side = right).
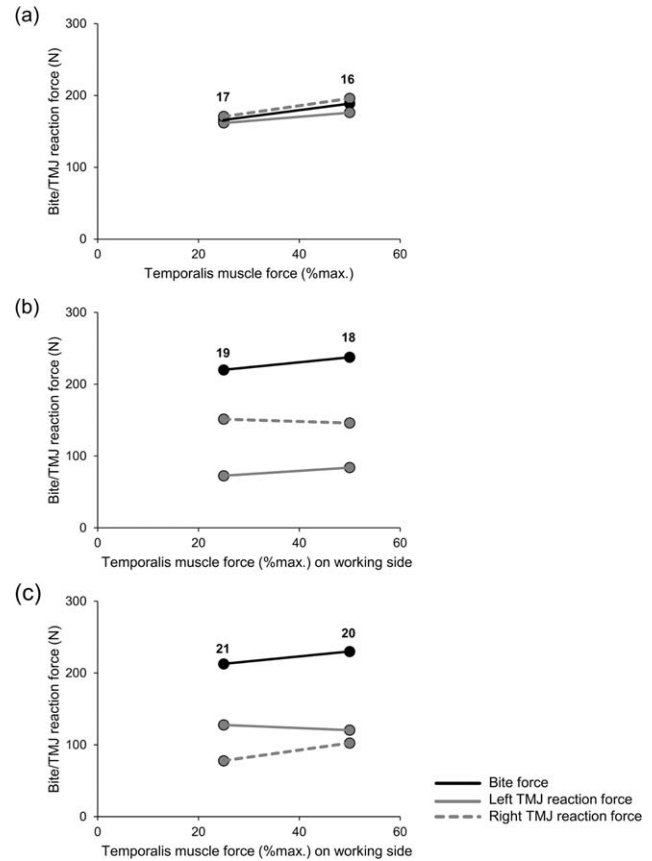

Fig. 5. Loadcases simulating heterogeneously activated muscles. Bite forces and TMJ reaction forces are plotted against the percentage of maximum temporalis force acting on the working side. Loadcase number is shown in bold. (a) I[1] bites, (b) left M[1] bites (working side = left), and (c) right M[1] bites (working side = right).
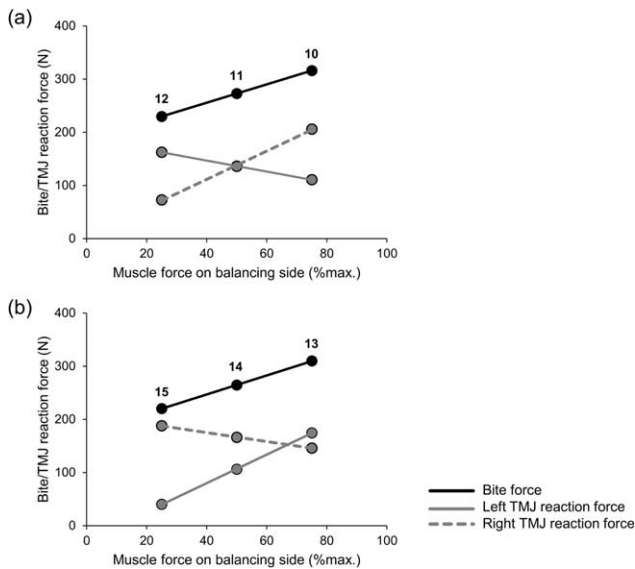

Fig. 4. Bite forces and TMJ reaction forces in loadcases simulating asymmetric, homogeneously activated muscles. Loadcase number is shown in bold. (a) Left M[1] bite (working side = left), (b) right M[1] bite (working side = right).

and 2) show an approximately linear relationship with total applied muscle force. This is in agreement with the results of Ross et al. (2005) and Fitton et al. (2012) in macaque models and it is expected for linearly elastic materials.

Varying simulated muscle activation patterns has a small impact on strain distribution. Principally this affects the regions local to the masseter muscle attachment site, causing strains to vary in this region according to the force of masseter contraction. This finding of consistent strain distribution under different muscle loading regimens points to the possibility of performing reliable FEAs of living, archaeological and fossil hominin crania using simplified muscle activations (e.g., symmetrically applied maximal muscle forces). Estimates of these forces might be obtained from the literature or from related species, directly from muscle CSAs as in the present study, or from bony proxies. This last method of estimation is likely to be inaccurate (Antón, 1994; Toro-Ibacache et al., 2015). However, such inaccuracy likely will impact strain magnitudes but not relative facial strains. Thus, if relative rather than absolute strains are of interest, reasonable muscle activation patterns all produce approximately similar results insofar as they apply similar total force.
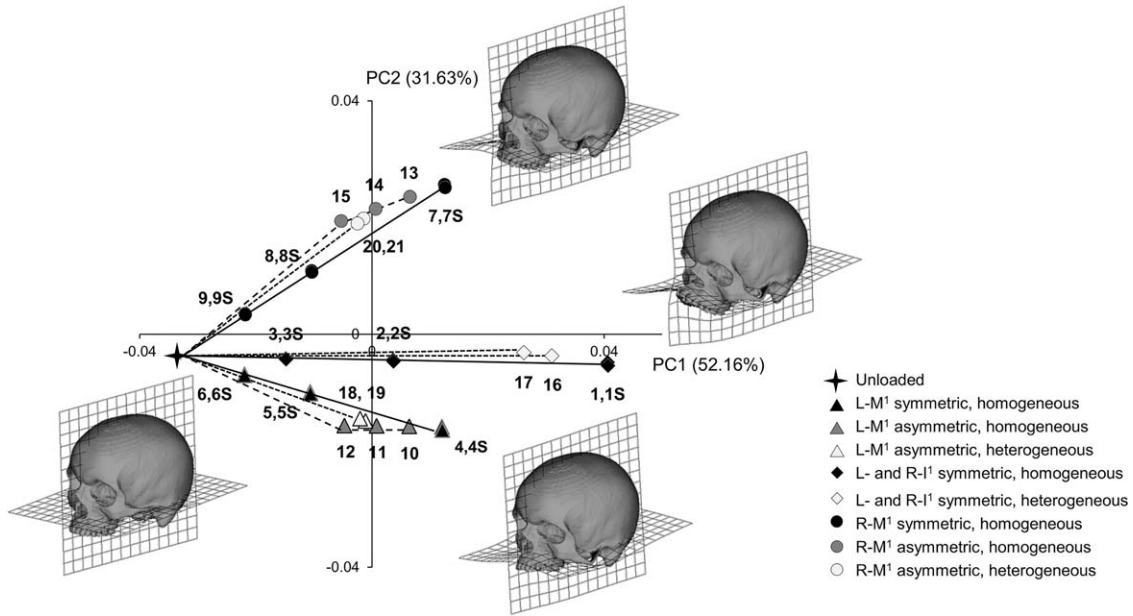
Fig. 6. Principal components analysis of 51 cranial landmarks on the unloaded model and the same model under different loadcases. The lines represent the vectors of deformation under each loading regimen. Loadcase numbers are shown in bold. S = loadcases with symmetric muscle force magnitudes, L = left and R = right. The inset surfaces with overlain transformation grids show: leftmost, the unloaded model; right upper, the largest deformation of the model resulting from right M[1] biting; right middle, the largest deformation resulting from I[1] biting; right lower, the largest deformation of the model resulting from left M[1] biting, all with the degree of deformation magnified 1,000 times for visualisation.
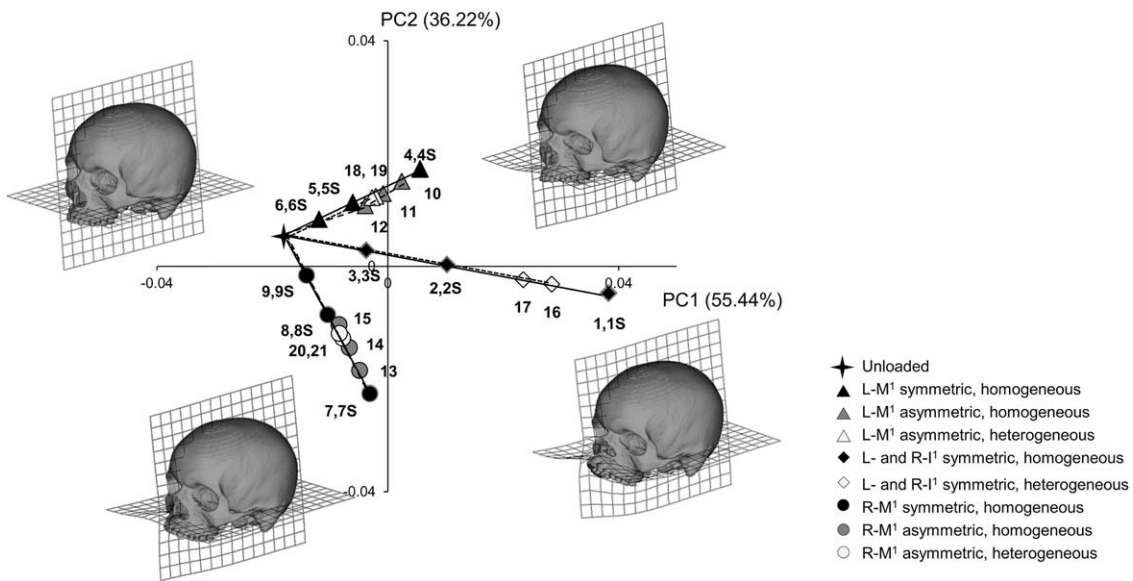

Fig. 7. Principal components analysis of 43 cranial landmarks on the unloaded model and the same model under different loadcases. Landmarks on the zygomatic arch are not included. The lines represent the vectors of deformation under each loading regimen. Loadcase numbers are shown in bold. S = loadcases with symmetric muscle force magnitudes, L = left and R = right. The inset surfaces with overlain transformation grids show: leftmost, the unloaded model; right upper, the largest deformation of the model resulting from left M[1] biting; right middle, the largest deformation resulting from I[1] biting; right lower, the largest deformation of the model resulting from right M[1] biting, all with the degree of deformation magnified 1,000 times for visualisation.

The present study varied relative force magnitudes but not muscle orientations. Each muscle was considered to have a single vector of action. This was a necessary simplification given the resolution of the CT images, since the finer details of muscle anatomy and fiber directions are not known. It is worth noting in this regard

that subdividing for example, the masseter into different parts with different vectors may introduce significant errors in estimation of the principal vector of muscle action (Röhrle and Pullan, 2007). The effect of varying the directions of muscle force vectors is worth exploring in future studies, especially where only the cranium is available and the position of mandibular muscle insertions has to be estimated. It is likely that such variations of vectors will principally impact modes of deformation.

Bite Force and TMJ Reaction Force

As expected with strain magnitudes, predicted bite force is proportional to total applied muscle force (Table 3). The same occurs with TMJ reaction forces during I^1 bites. During I^1 biting, small asymmetries in TMJ reaction forces can be observed, which is expected given the normal asymmetry of the skull.

Temporomandibular joint loading is an important human masticatory functional parameter; altered load distribution during mastication may result in dysfunction due to morphological changes and an inflammatory response in the articular tissues (McNamara, 1975; Tanaka et al., 2008; Barton, 2012). Temporomandibular joint loading in humans is difficult to estimate due to the impracticality of using direct methods and also because the mathematical models used to predict it have been shown to be highly sensitive to variations in muscle parameters (Throckmorton, 1985; Koolstra et al., 1988). Nevertheless, today it is generally acknowledged that during unilateral bites, the TMJ of the balancing side is more loaded than that of working side (Hylander, 1975; Throckmorton and Throckmorton, 1985; Koolstra and van Eijden, 2005; Shi et al., 2012). In this study such differences in loading between working and balancing sides are achieved during symmetric or close to symmetric muscle activations. However, under unilateral bites a much greater asymmetry (irrespective of heterogeneity) in muscle activations reverses the relationship between TMJ reaction forces at the working and balancing sides (Fig. 3). The sensitivity of TMJ reaction forces in the FE model to asymmetries in simulated muscle activations calls for further investigation using for example, multibody dynamic approaches (Curtis, 2011; Shi et al., 2012) to better understand the apparent reversal of TMJ reaction forces.

Considering these results, symmetrical maximum muscle forces appear to be a reasonable simplification approach in FEAs of the human cranium as long as relative rather than absolute strain magnitudes are of interest.

Global Model Deformation

As with predicted strains and bite forces, for each simulated bite point, varying the muscle activation pattern mainly produces differences in the magnitude rather than mode of global model deformation of the cranium as assessed by PCA of size and shape coordinates. This magnitude relates to the total applied muscle force and reflects the linear relationship between load and deformation in isotropic linear elastic materials (as bone and teeth are modelled here), and is consistent with the findings of O'Higgins and Milne (2013) in femora.

That asymmetric muscle activations principally impact on zygomatic arch deformation is consistent with the findings of Fitton et al. (2012) who also noted that varying muscle activations mainly led to differences in the degree of zygomatic arch deformation. Principally this affects the regions local to the masseter muscle attachment site. We found that ignoring zygomatic landmarks in the size and shape analysis results in vectors of deformation that closely overlap for each bite point, irrespective of muscle activation pattern. This may reflect a physiological, greater sensitivity of the zygomatic region to varying muscle force or it may be a consequence of inadequate representation of the temporal fascia (Curtis et al., 2011). The present study is uninformative in this regard. However, removing zygomatic arch landmarks does not affect the way model deformation in the face is depicted: dorsal bending of the maxilla during I^1 bites and apical-buccal deformation of the tooth and its alveolar bone during M^1 bites.

CONCLUSION

The results of this study show that the main effect of varying relative magnitudes of applied muscle forces on the FE model of a human cranium during simulated biting concerns the scaling of deformation (local strains and global size and shape change) and bite force with total applied muscle force. The effect on mode of deformation is much smaller, principally impacting on the zygomatic arch, where masseter attaches. TMJ reaction forces seem to be sensitive to symmetry of loading of the masticatory system

The hypothesis that varying the relative magnitudes of muscle forces during the same biting task has no effect on FEA results in terms of strain distribution and magnitude, bite force, TMJ reaction force and global model deformation was falsified. Thus, while modes of deformation (as assessed by strain distributions and the size and shape PCA) are relatively unaltered, the magnitudes of deformation vary with total applied muscle force as might be expected. Likewise, and as expected, bite force covaries with total applied muscle force. On the other hand, the relative magnitudes of left and right TMJ reaction forces are sensitive to applied muscle forces, especially asymmetry of these forces.

Considering these findings, when relative strain magnitudes among cranial regions are the focus of interest, the use of symmetric maximum muscle forces is a reasonable loading simplification. However the degree of deformation and so, magnitudes of strains are unlikely to be accurately predicted unless accurate muscle forces are applied. This is of particular relevance in the study of archaeological material and fossil hominins, where no muscle data are available.

LITERATURE CITED

Antón SC. 1990. Neandertals and the anterior dental loading hypothesis: a biomechanical evaluation of bite force production. Kroeber Anthropol Soc Pap 71/72:67–76.

Antón SC. 1994. Masticatory muscle architecture and bone morphology in primates. Berkeley: University of California.

Antón SC. 1999. Macaque masseter muscle: internal architecture, fiber length and cross-sectional area. Int J Primatol 20:441–462.

Barton ER. 2012. Mechanical signal transduction: divergent communication and the potential consequences for masticatory muscle. Semin Orthod 18:2–9.

Blanksma N, van Eijden T. 1995. Electromyographic heterogeneity in the human temporalis and masseter muscles during static biting, open\close excursions, and chewing. J Dent Res 74:1318–1327.

Bright JA. 2012. The importance of craniofacial sutures in biomechanical finite element models of the domestic pig. PLoS One 7:e31769.

Bright JA, Gröning F. 2011. Strain accommodation in the zygomatic arch of the pig: a validation study using digital speckle pattern interferometry and finite element analysis. J Morphol 272:1388–1398.

Curtis N. 2011. Craniofacial biomechanics: an overview of recent multibody modelling studies. J Anat 218:16–25.

Curtis N, Witzel U, Fitton LC, O'higgins P, Fagan MJ. 2011. The mechanical significance of the temporal fasciae in *Macaca fascicularis*: an investigation using finite element analysis. Anat Rec 294:1178–1190.

Demes B. 1987. Another look at an old face: biomechanics of the Neandertal facial skeleton reconsidered. J Hum E 16:297–303.

Demes B, Creel N. 1988. Bite force, diet, and cranial morphology of fossil hominids. J Hum E 17:657–670.

Fagan MJ, Curtis N, Dobson CA, Karunanayaje JH, Kupczik K, Moazen M, Page L, Phillips R, O'Higgins P. 2007. Voxel-based finite analysis—working directly with MicroCT scan data. J Morphol 268:1071.

Farella M, Palumbo A, Milani S, Avecone S, Gallo L, Michelotti A. 2009. Synergist coactivation and substitution pattern of the human masseter and temporalis muscles during sustained static contractions. Clin Neurophysiol 120:190–197.

Ferrario V, Sforza C, Colombo A, Ciusa V. 2000. An electromyographic investigation of masticatory muscles symmetry in normo-occlusion subjects. J Oral Rehabil 27:33–40.

Fitton LC, Prôa M, Rowland C, Toro-Ibacache V, O'Higgins P. 2015. The impact of simplifications on the performance of a finite element model of a *Macaca fascicularis* cranium. Anat Rec 298:107–121.

Fitton LC, Shi JF, Fagan MJ, O'Higgins P. 2012. Masticatory loadings and cranial deformation in *Macaca fascicularis*: a finite element analysis sensitivity study. J Anat 221:55–68.

Gröning F, Fagan M, O'Higgins P. 2011. The effects of the periodontal ligament on mandibular stiffness: a study combining finite element analysis and geometric morphometrics. J Biomech 44:1304–1312.

Gross MD, Arbel G, Hershkovitz I. 2001. Three-dimensional finite element analysis of the facial skeleton on simulated occlusal loading. J Oral Rehabil 28:684–694.

Hagberg C, Agerberg G, Hagberg M. 1985. Regression analysis of electromyographic activity of masticatory muscles versus bite force. Eur J Oral Sci 93:396–402.

Hylander WL. 1975. The human mandible: lever or link? Am J Phys Anthropol 43:227–242.

Jansen van Rensburg GJ, Wilke DN, Kok S. 2012. Human skull shape and masticatory induced stress: Objective comparison through the use of non-rigid registration. Int J Numer Method Biomed Eng 28:170–185.

Koolstra J, Tanaka E. 2009. Tensile stress patterns predicted in the articular disc of the human temporomandibular joint. J Anat 215:411–416.

Koolstra J, van Eijden T. 2005. Combined finite-element and rigid-body analysis of human jaw joint dynamics. J Biomech 38:2431–2439.

Koolstra J, van Eijden T, Weijs W, Naeije M. 1988. A three-dimensional mathematical model of the human masticatory system predicting maximum possible bite forces. J Biomech 21:563–576.

Kupczik K. 2008. Virtual biomechanics: basic concepts and technical aspects of finite element analysis in vertebrate morphology. J Anthropol Sci 86:193–198.

Kupczik K, Dobson CA, Crompton RH, Phillips R, Oxnard CE, Fagan MJ, O'Higgins P. 2009. Masticatory loading and bone adaptation in the supraorbital torus of developing macaques. Am J Phys Anthropol 139:193–203.

Kupczik K, Dobson CA, Fagan MJ, Crompton RH, Oxnard CE, O'Higgins P. 2007. Assessing mechanical function of the zygomatic region in macaques: validation and sensitivity testing of finite element models. J Anat 210:41–53.

Liu J, Shi J, Fitton LC, Phillips R, O'Higgins P, Fagan MJ. 2012. The application of muscle wrapping to voxel-based finite element models of skeletal structures. Biomech Model Mechan 11:35–47.

McNamara J. 1975. Functional adaptations in the temporomandibular joint. Dent Clin N Am 19:457.

Moore CA, Smith A, Ringel RL. 1988. Task-specific organization of activity in human jaw muscles. J Speech Lang Hear R 31:670.

O'Connor CF, Franciscus RG, Holton NE. 2005. Bite force production capability and efficiency in Neandertals and modern humans. Am J Phys Anthropol 127:129–151.

O'Higgins P, Cobb SN, Fitton LC, Gröning F, Phillips R, Liu J, Fagan MJ. 2011. Combining geometric morphometrics and functional simulation: an emerging toolkit for virtual functional analyses. J Anat 218:3–15.

O'Higgins P, Fitton LC, Phillips R, Shi J, Liu J, Gröning F, Cobb SN, Fagan MJ. 2012. Virtual functional morphology: novel approaches to the study of craniofacial form and function. Evol Biol 39:521–535.

O'Higgins P, Milne N. 2013. Applying geometric morphometrics to compare changes in size and shape arising from finite elements analyses. Hystrix 24:126–132.

Prum G, Ten Bosch J, De Jongh H. 1978. Jaw muscle EMG-activity and static loading of the mandible. J Biomech 11:389–395.

Rayfield EJ. 2007. Finite element analysis and understanding the biomechanics and evolution of living and fossil organisms. Annu Rev Earth Planet Sci 35:541–576.

Reaz MB, Hussain M, Mohd-Yasin F. 2006. Techniques of EMG signal analysis: detection, processing, classification and applications. Biol Proced Online 8:11–35.

Richmond BG, Wright BW, Grosse I, Dechow PC, Ross CF, Spencer MA, Strait DS. 2005. Finite element analysis in functional morphology. Anat Rec 283:259–274.

Ross CF, Berthaume MA, Dechow PC, Iriarte-Diaz J, Porro LB, Richmond BG, Spencer M, Strait D. 2011. *In vivo* bone strain and finite-element modeling of the craniofacial haft in catarrhine primates. J Anat 218:112–141.

Ross CF, Patel BA, Slice DE, Strait DS, Dechow PC, Richmond BG, Spencer MA. 2005. Modeling masticatory muscle force in finite element analysis: sensitivity analysis using principal coordinates analysis. Anat Rec 283:288–299.

Schindler HJ, Rues S, Türp JC, Schweizerhof K, Lenz J. 2005. Activity patterns of the masticatory muscles during feedback-controlled simulated clenching activities. Eur J Oral Sci 113:469–478.

Shi J, Curtis N, Fitton LC, O'Higgins P, Fagan MJ. 2012. Developing a musculoskeletal model of the primate skull: predicting muscle activations, bite force, and joint reaction forces using multibody dynamics analysis and advanced optimisation methods. J Theor Biol 310:21–30.

Smith AL, Benazzi S, Ledogar JA, Tamvada K, Pryor Smith LC, Weber GW, Spencer MA, Dechow PC, Grosse IR, Ross CF, et al. 2015a. Biomechanical implications of intraspecific shape variation in chimpanzee crania: moving toward an integration of geometric morphometrics and finite element analysis. Anat Rec 298:122–144.

Smith AL, Benazzi S, Ledogar JA, Tamvada K, Pryor Smith LC, Weber GW, Spencer MA, Lucas PW, Michael S, Shekeban A, et al.

2015b. The feeding biomechanics and dietary ecology of *Paranthropus boisei*. Anat Rec 298:145–167.

Soderberg GL, Cook TM. 1984. Electromyography in biomechanics. Phys Ther 64:1813–1820.

Spencer MA. 1998. Force production in the primate masticatory system: electromyographic tests of biomechanical hypotheses. J Hum E 34:25–54.

Stohler C. 1986. A comparative electromyographic and kinesiographic study of deliberate and habitual mastication in man. Arch Oral Biol 31:669–678.

Strait DS, Wang Q, Dechow PC, Ross CF, Richmond BG, Spencer MA, Patel BA. 2005. Modeling elastic properties in finite-element analysis: how much precision is needed to produce an accurate model? Anat Rec 283:275–287.

Strait DS, Weber GW, Neubauer S, Chalk J, Richmond BG, Lucas PW, Spencer MA, Schrein C, Dechow PC, Ross CF. 2009. The feeding biomechanics and dietary ecology of *Australopithecus africanus*. Proc Natl Acad Sci USA 106:2124–2129.

Tanaka E, Detamore M, Mercuri L. 2008. Degenerative disorders of the temporomandibular joint: etiology, diagnosis, and treatment. J Dent Res 87:296–307.

Tanne K, Miyasaka J, Yamagata Y, Sachdeva R, Tsutsumi S, Sakuda M. 1988. Three-dimensional model of the human craniofacial skeleton: method and preliminary results using finite element analysis. J Biomed Eng 10:246–252.

Throckmorton GS. 1985. Quantitative calculations of temporomandibular joint reaction forces—II. The importance of the direction of the jaw muscle forces. J Biomech 18:453–461.

Throckmorton GS, Throckmorton LS. 1985. Quantitative calculations of temporomandibular joint reaction forces—I. The importance of the magnitude of the jaw muscle forces. J Biomech 18:445–452.

Toro-Ibacache V, Fitton LC, Fagan MJ, O'Higgins P. 2016a. Validity and sensitivity of a human cranial finite element model: implications for comparative studies of biting performance. J Anat 228:70–84.

Toro-Ibacache V, Zapata Muñoz V, O'Higgins P. 2015. The predictability from skull morphology of temporalis and masseter muscle cross-sectional areas in humans. Anat Rec 298:1261–1270.

Toro-Ibacache V, Zapata Muñoz V, O'Higgins P. 2016b. The relationship between skull morphology, masticatory muscle force and cranial skeletal deformation during biting. Ann Anat 203:59–68.

Ueda HM, Ishizuka Y, Miyamoto K, Morimoto N, Tanne K. 1998. Relationship between masticatory muscle activity and vertical craniofacial morphology. Angle Orthod 68:233–238.

van Eijden T. 1990. Jaw muscle activity in relation to the direction and point of application of bite force. J Dent Res 69:901–905.

van Eijden T, Korfage J, Brugman P. 1997. Architecture of the human jaw-closing and jaw-opening muscles. Anat Rec 248:464–474.

van Spronsen P, Weijs W, Valk J, Prahl-Andersen B, van Ginkel F. 1991. Relationships between jaw muscle cross-sections and craniofacial morphology in normal adults, studied with magnetic resonance imaging. Eur J Orhod 13:351–361.

Vitti M, Basmajian JV. 1977. Integrated actions of masticatory muscles: simultaneous EMG from eight intramuscular electrodes. Anat Rec 187:173–189.

Wang K, Arima T, Arendt-Nielsen L, Svensson P. 2000. EMG–force relationships are influenced by experimental jaw-muscle pain. J Oral Rehabil 27:394–402.

Weijs W, Hillen B. 1984. Relationship between the physiological cross-section of the human jaw muscles and their cross-sectional area in computer tomograms. Acta Anat 118:129–138.

Weijs W, Hillen B. 1985. Cross-sectional areas and estimated intrinsic strength of the human jaw muscles. Acta Morphol Neer Sc 23:267–274.

Weijs W, Hillen B. 1986. Correlations between the cross-sectional area of the jaw muscles and craniofacial size and shape. Am J Phys Anthropol 70:423–431.

Wood SA, Strait DS, Dumont ER, Ross CF, Grosse IR. 2011. The effects of modeling simplifications on craniofacial finite element models: The alveoli (tooth sockets) and periodontal ligaments. J Biomech 44:1831–1838.

Wroe S, Ferrara TL, McHenry CR, Curnoe D, Chamoli U. 2010. The craniomandibular mechanics of being human. Proc R Soc B 277:3579–3586.